Eddy-Current Computation in the Claws of a Synchronous Claw-Pole Alternator in Generator Mode

Christian Kaehler and Gerhard Henneberger

***Abstract*—This paper deals with the three-dimensional finite-element (FE) calculation of eddy currents in the claws of a claw-pole alternator taking the rotational geometry movement into account. For this calculation a transient edge-based $\vec{A}$, $\vec{A}-\vec{T}$ formulation is utilized. The generation of the FE model with a special focus on the discretization of eddy-current regions and air gap is presented. The main intention lies in determining the eddy-current losses in the rotor claws in generator mode at constant speed. Since high-speed and high material conductivity leads to divergence, underrelaxation of the material conductivity in the claws is conducted.**

***Index Terms*—Eddy currents, finite-element calculations, rotating machines, transient lock step method.**

I. Introduction

CLAW-POLE alternators are used for generation of electricity in automobiles. There are three basic requirements to them: The output performance must be improved, the audible noise reduced, and the efficiency increased. A description of the magneto-static field calculation, used for output optimization and the analysis of the structural-dynamic and acoustic behavior, can be found in [1], [2].

The efficiency of machines is decreased by different loss mechanisms. In the case of the claw-pole alternator, these are dominantly ohmic losses in the coils and losses caused by eddy currents in conducting materials. Both can be broken down into rotor and stator parts. Whereas the ohmic losses can be directly calculated in dependence of the coil currents, an analytic description of eddy-current losses is not possible. Measurements of the total loss in combination with a subtraction of all analytically defined loss mechanisms lead to a separation of eddy-current losses [3]. These show a rise in the ratio of eddy current to ohmic losses with higher speeds. The rotor claws are press-formed out of solid metal. Therefore, the eddy-current distribution in the claws is especially significant.

Using the finite element method (FEM), it is possible to calculate the eddy currents in conducting materials which are induced by an alternating magnetic field. A time-harmonic approach can be applied when the geometry is not shifting, all material properties are linear and sinusoidal currents are used. In the case of the claw-pole synchronous machine, the rotor is turning with a defined speed while direct current is used in the excitation coil of the rotor. In generator mode, the stator coils are driven by three-phase current. Therefore, a time-stepping algorithm has to be utilized. The main advantages and disadvantages of this approach applied to the claw-pole alternator have already been discussed in [3].

In this paper, the applied transient edge-based $\vec{A}$, $\vec{A}-\vec{T}$ approach in eddy-current regions is outlined [4]. The three-dimensional (3-D) FE-model of the claw-pole alternator and calculation results at load in generator mode at constant speed of $n = 1800$ rpm, $n = 2400$ rpm, $n = 3000$ rpm, and $n = 4500$ rpm with varying material conductivity in the claw regions are presented.

II. Theory of Edge-Based Solver

The applied edge-based solver uses the FE eddy-current formulation presented in [4]. Two vector potentials, the magnetic vector potential $\vec{A}$ and the electric vector potential $\vec{T}$, are used to compute the flux density $\vec{B}$ and the current density $\vec{J}$

$$\nabla \times \vec{A} = \vec{B}, \qquad \nabla \times \vec{T} = \vec{J}. \tag{1}$$

The solver separates the model in eddy-current-free regions Ω_1, where the following equation for $\vec{A}$ is solved:

$$\int_{\Omega_1} \nabla \times \vec{\alpha}_i \cdot \nu \nabla \times \vec{A}(t) d\Omega_1 = \int_{\Omega_1} \left(\vec{\alpha}_i \cdot \vec{J}_0(t) + \nabla \times \vec{\alpha}_i \cdot \nu \vec{B}_r \right) d\Omega_1 \tag{2}$$

and eddy-current regions Ω_2, where the equations read

$$\int_{\Omega_2} \left(\nabla \times \vec{\alpha}_i \cdot \nu \nabla \times \vec{A}(t) - \vec{\alpha}_i \cdot \nabla \times \vec{T}(t) \right) d\Omega_2 = 0 \quad \wedge$$
$$\int_{\Omega_2} \left(\nabla \times \vec{\alpha}_i \cdot \frac{1}{\sigma} \nabla \times \vec{T}(t) + \nabla \times \vec{\alpha}_i \cdot \frac{\partial}{\partial t} \vec{A}(t) \right) d\Omega_2 = 0. \tag{3}$$

$\vec{J}_0(t)$ describes the given coil current density while $\vec{B}_r$ defines remanences. The material parameters ν and σ represent the nonlinear reluctivity and the linear conductivity. $\vec{\alpha}_i$ defines the shape function of an edge element (in this solver tetrahedrons).

The time-stepping algorithm interpolates the time-dependent variables linearly as follows:

$$\vec{A}(t) = \tau \cdot \vec{A}_{n+1} + (1-\tau)\vec{A}_n \quad \text{ditto for } \vec{T},\ \vec{J}_0 \tag{4}$$

Manuscript received July 15, 2001; revised October 25, 2001.

The authors are with the Department of Electrical Machines (IEM), Aachen Institute of Technology (RWTH), D-52056 Aachen, Germany (e-mail: christian.kaehler@iem.rwth-aachen.de).

Publisher Item Identifier S 0018-9464(02)01228-1.

$$\frac{\partial}{\partial t}\vec{A}(t) = \frac{1}{\Delta t}\left(\vec{A}_{n+1} - \vec{A}_n\right), \tag{5}$$

where the index n represents the number of the transient step and Δt the time in between transient steps.

In order to get better convergence behavior, the scaled current potential $\vec{T}^{\diamond}$ is applied

$$\vec{T}^{\diamond} = -\frac{\Delta t}{\sigma}\vec{T} \tag{6}$$

leading to the following equation set for eddy-current-free regions (Ω_1):

$$\int_{\Omega_1} \nabla\times\vec{\alpha}_i\cdot\nu\nabla\times\left[\tau\vec{A}_{n+1}+(1-\tau)\vec{A}_n\right]\,d\Omega_1 = \int_{\Omega_1}\left(\alpha_i\cdot\left[\tau\vec{J}_{0,n+1}+(1-\tau)\vec{J}_{0,n}\right]+\nabla\times\alpha_i\cdot\nu\vec{B}_r\right)\,d\Omega_1 \tag{7}$$

and eddy-current regions (Ω_2)

$$\begin{aligned}\int_{\Omega_2}&\left(\nabla\times\vec{\alpha}_i\cdot\nu\nabla\times\left[\tau\vec{A}_{n+1}+(1-\tau)\vec{A}_n\right]\right.\\ &\left.+\vec{\alpha}_i\cdot\frac{\sigma}{\Delta t}\nabla\times\left[\tau\vec{T}^{\diamond}_{n+1}+(1-\tau)\vec{T}^{\diamond}_{n}\right]\right)\,d\Omega_2 = 0\\ \wedge\quad&\int_{\Omega_2}\left(\nabla\times\vec{\alpha}_i\cdot\frac{1}{\Delta t}\nabla\times\left[\tau\vec{T}^{\diamond}_{n+1}+(1-\tau)\vec{T}^{\diamond}_{n}\right]\right.\\ &\left.+\nabla\times\vec{\alpha}_i\cdot\frac{1}{\Delta t}\left(\vec{A}_{n+1}-\vec{A}_n\right)\right)\,d\Omega_2 = 0.\end{aligned} \tag{8}$$

The usual periodic and Dirichlet boundary conditions are used on the model boundaries for $\vec{T}$ and $\vec{A}$. The boundary condition between eddy-current-free regions Ω_1 and eddy-current regions Ω_2 for the current vector potential reads [5]

$$\Gamma_{12}: \quad \vec{T}\times\vec{n} = 0 \tag{9}$$

where $\vec{n}$ is the normal vector of the region boundary.

Since in this application all eddy-current regions are continuous and short circuited, (9) can easily be achieved by a Dirichlet condition $T_i = 0$ on all edges i of the boundary Γ_{12}.

The global matrix is solved by a stabilized Gauss BCG solver of the ITL-Package [6]. Saturation effects are computed with an overlaying Newton–Raphson procedure for each transient step. The relaxation factor used in between transient steps is chosen as $\tau = 2/3$ (Galerkin-scheme).

III. Finite Element Model

The magnetically relevant components of the synchronous claw-pole alternator are modeled (Fig. 1). Since the geometry of the alternator is symmetric over two pole pitches, only a 60° model is generated and periodic boundaries are defined.

The winding head is simplified as depicted in Fig. 2. Thus, the synchronous alternator with 36 stator teeth (number of pole pairs $p = 6$) is reduced to a machine whose geometry and electro-magnetic field distribution is periodic after a rotation of one stator tooth pitch (i.e., $360°/p\cdot 2\cdot 3 = 10°$) of its rotor instead of the 60° periodicity with regular winding heads.

In order to discretize the penetration depth of the eddy currents and achieve low Peclet numbers [7], the surfaces of the eddy-current regions have to be meshed very densely (Fig. 1, rotor claws). A useful mesh density would be two to three element layers within the penetration depth. Due to the large element numbers of the 3-D model, this is not possible with respect to calculation time and available memory. Instead, about one and a half element layers are used, leading to an overall element count of around 390 000.

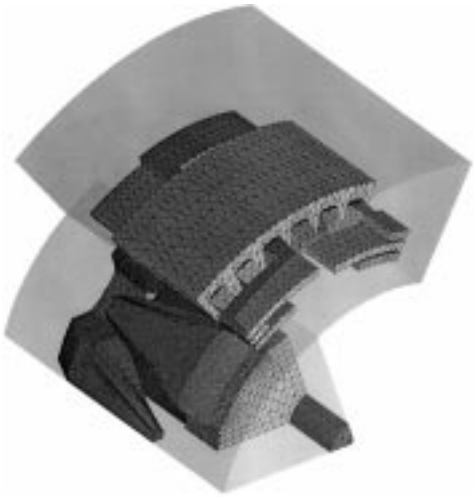

Fig. 1. Discretized FE model with translucent air regions.

Fig. 2. Simplified winding region.

To represent the rotational movement, a lock-step method is utilized. In this method, no real movement takes place. Instead, boundary conditions are used which pair adjoining edges in each step depending on the rotational angle, while the mesh remains stationary.

This edge reordering routine of the transient solver needs a special air gap discretization. To implement the change of geometry, the FE-mesh of the alternator is separated into moving elements in the rotor and stationary elements in the stator. The boundary area of these two meshes is located in the middle of the air gap. The boundary area is meshed identically in both separate meshes. This boundary mesh is partitioned into equidistant areas in the direction of movement, which have to be meshed absolutely identical again, so that the reordering routine can pair two edges in each transient step [4].

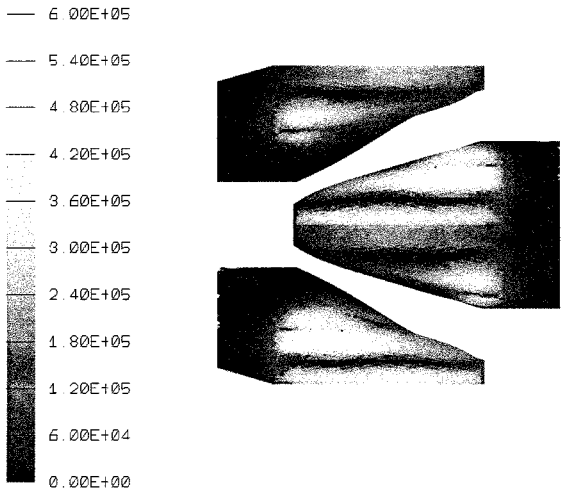

Fig. 3. Eddy-current-density distribution $(\mathrm{A/m^2})$ on the rotor claws at speed $n = 4500$ rpm and conductivity $\sigma = 4.0 \cdot 10^4 (1/\Omega\mathrm{m})$.

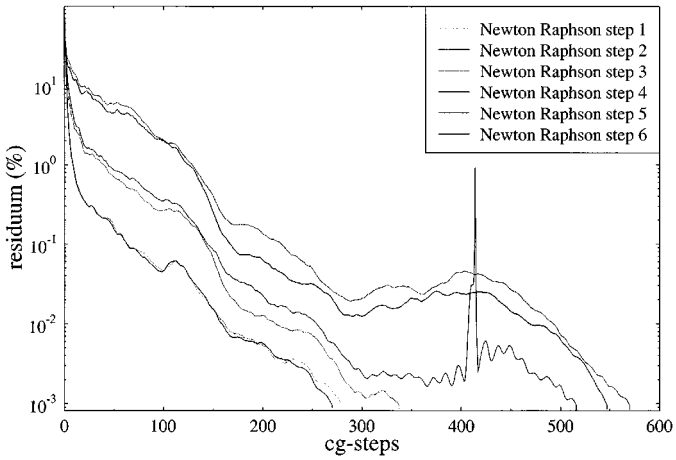

Fig. 4. Convergence history for low material conductivity.

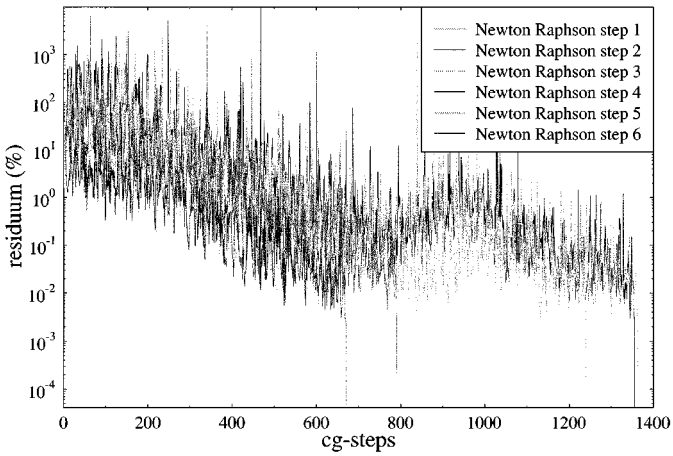

Fig. 5. Convergence history for high material conductivity.

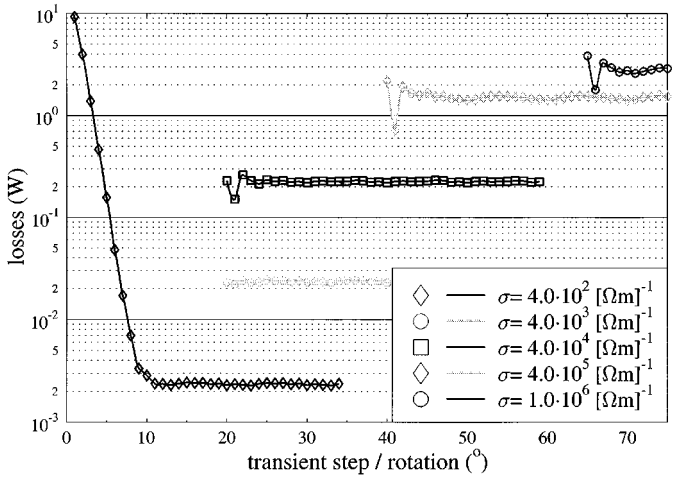

Fig. 6. Eddy-current losses versus rotation for various material conductivities at constant speed $n = 1800$ rpm.

IV. Calculations and Results

The calculations are conducted at constant speed. The mechanical step angle amounts to $\alpha = 1°$, leading to e.g., $\Delta t = 55.556\ \mu$s in between transient steps for a speed of $n = 3000$ rpm. The excitation current is impressed in the rotor. The three-phase current of the real alternator in generator mode is injected in the stator coils. It turns synchronously with the rotor.

In order to achieve smooth convergence and to reduce the settling time, the calculation is started with the material conductivity of the claws being $\sigma = 4.0 \cdot 10^2 (1/\Omega\mathrm{m})$ or Peclet number $P_e \approx 0.001$, which is defined as [7]

$$P_e = \frac{v \cdot l \cdot \mu \cdot \sigma}{2}. \tag{10}$$

In (10), v represents the velocity, l is the characteristic length of an element in the direction of movement, and μ is the permeability of the element material. The conductivity is subsequently increased to $\sigma = 4.0 \cdot 10^3 (1/\Omega\mathrm{m})$, $\sigma = 4.0 \cdot 10^4 (1/\Omega\mathrm{m})$, $\sigma = 4.0 \cdot 10^5 (1/\Omega\mathrm{m})$, and $\sigma = 1.0 \cdot 10^6 (1/\Omega\mathrm{m})$ or $P_e \approx 2.5$. The real conductivity of $\sigma = 4.0 \cdot 10^6 (1/\Omega\mathrm{m})$ leads to divergence ($P_e \approx 10$). Therefore, the simulation is finished with a material conductivity, which is factor four lower than the real conductivity of the claws.

Consequently, while the eddy-current distribution (Fig. 3) does not change qualitatively when varying high material conductivity, the calculated values of the total eddy-current losses in the claws are too low.

The convergence histories for a comparable time step, identical speed, and different material conductivities show the influence of the conductivity on the stability of the matrix system. Fig. 4 depicts the convergence history at a relatively low conductivity of $\sigma = 4.0 \cdot 10^3 (1/\Omega\mathrm{m})$. The convergence does not differ relevantly from static convergence although oscillations appear around cg-step 400. In contrast, at $\sigma = 1.0 \cdot 10^6 (1/\Omega\mathrm{m})$ the oscillations dominate the convergence behavior (Fig. 5).

The total eddy-current losses in the claws over the rotation is depicted in Fig. 6. After a short settling time of about ten time steps, a periodicity of the eddy-current losses of $\Delta\alpha = 10°$ mechanical establishes. To emphasize this periodicity, a zoom on the losses at material conductivity $\sigma = 4.0 \cdot 10^5 (1/\Omega\mathrm{m})$ is depicted in Fig. 7. The periodicity is congruent with the assumptions taken in Section III.

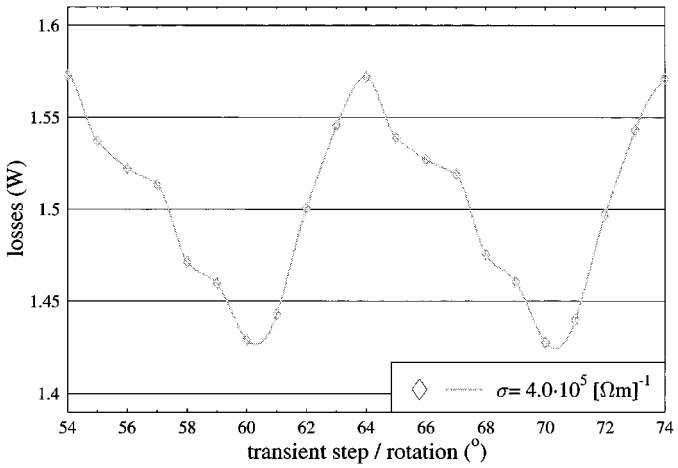

Fig. 7. Zoom on eddy-current losses versus rotation for a specific material conductivity at constant speed $n = 1800$ rpm.

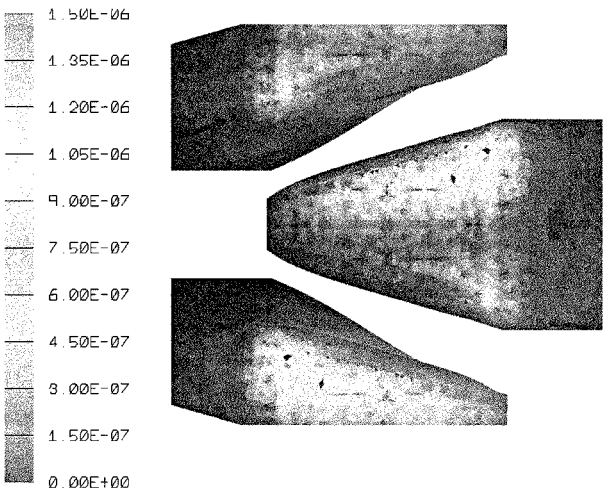

Fig. 8. Average eddy-current loss energy (Ws) at material conductivity $\sigma = 4.0 \cdot 10^4 (1/\Omega\mathrm{m})$ and constant speed $n = 4500$ rpm.

Taking the average eddy-current loss energy for each element

$$\overline{W} = \frac{\Delta t \cdot V}{\sigma} \cdot \sum_{n=1}^{N} \vec{J}_n^2, \tag{11}$$

with N being the number of steps in a period, V the volume of an element, and $\vec{J}_n$ the eddy-current density of that element at step n, over a period of the losses leads to Fig. 8. The distribution of the average loss energy can later be used as excitation for thermal solvers. Since the thermal distribution will only differ by diffusion effects from the energy distribution, the maxima distribution in Fig. 8 can already be compared to hotspot distributions in temperature measurements on the surfaces of the rotor claws.

By using the mean values of the calculations with low material conductivity (Table I), an extrapolation function can be constructed to compute the losses at the real conductivity

$$\frac{P_{\text{eddy currents}}}{[\mathrm{W}]} = f(\sigma) = m \cdot \left(\frac{\sigma}{\left[\frac{1}{\Omega\mathrm{m}}\right]} \right)^{x} \tag{12}$$

TABLE I
TOTAL EDDY CURRENT LOSSES IN ROTOR CLAWS (W) WITH WINDING HEADS AT SPEED $n = 3000$ RPM

Conductivity $(1/\Omega\mathrm{m})$	$4 \cdot 10^2$	$4 \cdot 10^4$	$4 \cdot 10^5$	$1 \cdot 10^6$	$4 \cdot 10^6$
Calculated losses	104 μ	7.02	30.66	50.1	
Extrapolated losses					112.8

TABLE II
CALCULATED TOTAL EDDY CURRENT LOSSES IN ROTOR CLAWS (W) WITH SIMPLIFIED WINDINGS, EXTRAPOLATION IN SQUARE BRACKETS

Conductivity $(1/\Omega\mathrm{m})$	$4 \cdot 10^2$	$4 \cdot 10^3$	$4 \cdot 10^4$	$4 \cdot 10^5$	$1 \cdot 10^6$	$4 \cdot 10^6$
$n = 1250$ rpm	7.36μ	72.6μ	714μ	5.95	[10.9]	[27.4]
$n = 3000$ rpm	14.1μ	141μ	1.35	9.00	16.5	[41.0]
$n = 3000$ rpm	47.8μ	471μ	3.90	16.9	[29.9]	[70.7]
$n = 4500$ rpm	114μ	1.1	7.07	27.3	[47.9]	[111]

with m and x being geometry-dependent parameters, which for the specific claw-pole alternator geometry described in this paper at a speed of $n = 3000$ rpm amount to $m = 3.25 \cdot 10^{-3}$ and the exponent $x = 0.57$.

Table II presents the calculated loss values with simplified winding heads combined with the extrapolated values in brackets.

V. CONCLUSION

In this paper, a 3-D FE method to calculate the eddy currents in the claws of a synchronous claw-pole alternator is presented taking the rotational movement into account. Although a computation with the real material conductivity is not possible due to convergence problems, an extrapolation of the eddy-current losses is shown. In addition, the eddy-current-density distribution as well as the average eddy-current loss energy distribution on the rotor claws with decreased material conductivity are depicted.

REFERENCES

[1] S. Küppers, "Numerische Verfahren zur Berechnung und Auslegung von Drehstrom–Klauenpolgeneratoren," Ph.D. dissertation, Department of Electrical Machines (IEM), Aachen Institute of Technology (RWTH), Aachen, Germany, 1996.

[2] M. Hecquet, S. Dahel, M. Goueygou, and P. Brochet, "Numerical determination of pole shape influence on radial forces in an automotive alternator," in *Proc. 2nd Int. Sem. Vibrations and Acoustic Noise of Electric Machinery (VANEM)*, Lodz, Poland, June 2000, pp. 39–43.

[3] C. Kaehler and G. Henneberger, "Three-dimensional eddy-current computation in the claws of a synchronous claw-pole alternator," presented at the 5th Int. Sem. Electric and Magnetic Fields (EMF), Ghent, Belgium, May 2000.

[4] D. Albertz and G. Henneberger, "On the use of the new edge-based $\vec{A}$, $\vec{A} - \vec{T}$ formulation for the calculation of time-harmonic, stationary and transient current field problems," *IEEE Trans. Magn.*, vol. 36, pp. 818–822, July 2000.

[5] O. Biro and K. Preis, "An edge finite element eddy-current formulation using a reduced magnetic and a current vector potential," *IEEE Trans. Magn.*, vol. 36, pp. 3128–3130, Sept. 2000.

[6] A. Lumsdaine and J. Siek. The iterative template library. [Online]. Available: http://www.lsc.nd.edu/research/itl

[7] D. Rodger, P. J. Leonhard, and T. Karaguler, "An optimal formulation for 3-D moving conductor eddy-current problems with smooth rotor," *IEEE Trans. Magn.*, vol. 26, pp. 2359–2363, Sept. 1990.